PAPER

Check for updates

Intimate ruthenium–platinum nanoalloys supported on carbon catalyze the hydrogenation and one-pot hydrogenation-coupling reaction of oxidized amino derivatives†

Miguel A. Rivero-Crespo, [iD] ‡[a] Paula Rubio-Marqués,§[a]
Juan Carlos Hernández-Garrido, [iD] [b] Marta Mon,[a]
Judit Oliver-Meseguer [iD] [a] and Antonio Leyva-Pérez [iD] *[a]

The use of bimetallic nanoparticles as catalysts in complex organic synthesis is rare, despite the widespread use of these materials in thermal C_1 chemistry and electrocatalysis. Here we show that intimate RuPt nanoalloys, supported on charcoal, catalyze the synthesis of secondary and tertiary amines from a variety of amino derivatives, such as quinolines, isoquinolines, nitrobenzenes, oximes and nitriles, under mild reaction conditions. The organic reactions include not only direct hydrogenation reactions but also hydrogen-borrowing couplings in cascade, to access the desired amines in one-pot from readily available materials. The recyclable bimetallic solid catalyst is at least one order of magnitude more active than the monometallic counterparts in some cases, which illustrates the advantages of Ru–Pt co-operation during hydrogenation and hydrogen-borrowing reactions.

Introduction

Alloyed bimetallic nanoparticles (nanoalloys) are now accessible to researchers and their use in a great variety of fields has rapidly increased during the last years.[1] A representative bimetallic combination is ruthenium–platinum (RuPt), well-known during years in nanoalloyed form, and with extensive use in thermo- and electro-catalysis, for instance for carbon monoxide oxidation,[2] hydrogen and oxygen evolution reactions (HER and OER),[3] methanol oxidation and fuel cell applications,[4] and hydrodeoxygenation reactions,[4g] among other reactions.[5] Related to this, RuNi nanoalloys have also been employed as catalysts.[6] In striking contrast, little use of RuPt nanoalloys has been done in more

[a] *Instituto de Tecnología Química (UPV-CSIC) Universitat Politècnica de València-Consejo Superior de Investigaciones Científicas, Avda. de los Naranjos s/n, 46022 Valencia, Spain. E-mail: anleyva@itq.upv.es*
[b] *Departamento de Ciencia de los Materiales e Ingeniería Metalúrgica y Química Inorgánica, Facultad de Ciencias, Universidad de Cádiz, Campus Universitario Puerto Real, 11510 Puerto Real, Cádiz, Spain*
† Electronic supplementary information (ESI) available: Experimental section, Fig. S1–S13 and Tables S1–S7. See DOI: https://doi.org/10.1039/d2cy01846b
‡ Current address: Swiss Federal Institute of Technology (ETH), Zurich, Switzerland.
§ Current address: Pharmacoepidemiology and Pharmacovigilance Division, Medicines for Human Use Department, Spanish Agency for Medicines and Medical Devices (AEMPS), Madrid, Spain.

complex organic synthesis. To our knowledge, the selective hydrogenation of benzene to 1,4-cyclohexadiene[7a] and the reduction of phthalates[7b] have been some of the few reported examples with relatively complex organic reactions catalysed by RuPt nanoalloys.

Reactions involving the selective transferring of H atoms constitute an atom-efficient, economic and environmentally-friendly way to prepare new chemicals in organic synthesis.[8] Fig. 1 shows two examples with broad industrial application,[9] the classical Sabatier hydrogenation where H_2 is activated, dissociated and transferred on a metal surface catalyst; and the hydrogen-borrowing coupling reaction, where the metal catalyst first receives dissociated H atoms from the substrate and then gives them back, after the coupling of two substrate molecules.[10]

While the Sabatier reaction is commonly catalysed by Pt metal surfaces, the hydrogen-borrowing reaction is usually catalysed by Ru organometallic complexes; thus, the combination of both processes in one-pot with a single catalyst is not trivial.[11,12] If achieved, the potential use of oxidised amino derivatives as starting materials for the synthesis of alkyl amines, after incorporation of an unlimited amount of external H atoms, will open new synthetic opportunities.

It is well-known that Pt(0) nanoparticles rank among the most active catalysts for the dissociation and transfer of H_2 to unsaturated bonds such nitro and carbonyl derivatives,[13]

2508 | *Catal. Sci. Technol.*, 2023, **13**, 2508–2516

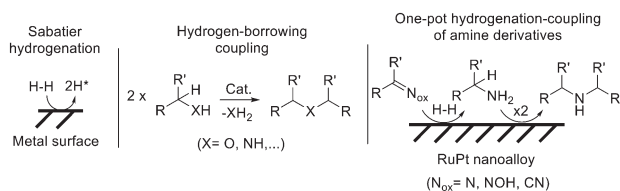This journal is © The Royal Society of Chemistry 2023

Fig. 1 Management of H atoms by metal catalysts during classical hydrogenation and hydrogen-borrowing reactions, and the combination of both. The three reactions are studied in this work for different amines, with RuPt nanoalloyed catalysts.

while low valence Ru complexes and nanoparticles are considered the most efficient catalysts for the hydrogenation of aromatics[14,15] and the deaminative coupling of amines.[16] Thus, it was envisioned here that a nanoparticle containing both Pt and Ru, intimately segregated, could catalyse in much better way than Pt and Ru, by separate, either the hydrogenation of amino-containing aromatic rings, the hydrogen-borrowing reaction of amines, or concomitantly both, enabling the one-pot hydrogenation–hydrogen-borrowing reaction of oxidized amine derivatives.[17] It is shown herein that, indeed, Ru–Pt nanoalloys catalyse the synthesis of secondary and tertiary alkyl amines after hydrogenation of quinolines, isoquinolines, nitrobenzenes, nitriles or imines, and also of aromatic rings, enabling amine or oxime hydrogen-borrowing couplings during the reaction.

Results and discussion

Synthesis and characterisation of the catalysts.

Ru–Pt nanoalloys with molar ratios 2:1, 1:1 and 1:3, on activated charcoal (RuPt–C), were prepared by impregnation of the support with an aqueous solution of the corresponding amounts of H_2PtCl_4 and $RuCl_3$. The total metal contain was typically kept in 5 wt%. The material was then dried at 100 °C and reduced under a H_2/N_2 flow (1:10) at 360 °C.[18] Inductively coupled plasma-atomic emission spectroscopy (ICP-AES), after treatment of the solids with strong acid aqueous solutions and filtration, confirmed that the total metal amount was incorporated and persisted onto the solid. For the sake of comparison, monometallic Ru–C and Pt–C samples were prepared by the same methodology. Fig. 2 shows high resolution transmission electron microscopy (HR-TEM) images of different samples of RuPt–C, with well-dispersed, homogeneous nanocrystallites present in the catalysts, and with an average size around 5 nm. Table 1 shows the particle diameter size values for the different samples of RuPt–C, as well as of the monometallic Ru–C and Pt–C materials, the latter presenting average sizes of d = 9.6 and 2.3 nm, respectively (Fig. S1†). Powder X-ray diffraction (XRD) analyses confirmed the relative average size of the nanoparticles, after applying the Scherrer equation (Fig. S2†).

Scanning transmission electron microscopy with annular dark field detector (STEM-DF) confirmed the metallic nature of the crystallites, and energy-dispersive X-ray spectroscopy (EDX) analysis, in Fig. 2D and E, shows that Ru and Pt are the only constituents of the nanocrystallites, and that both metals are intimately mixed at the sub-nanometer regime, since the signals of Ru and Pt are spatially coupled (see also Fig. S3†).

Scanning of some discrete particles in FESEM supports the presence of Ru and Pt in equal amounts in the 1:1 nanoalloy (Fig. S4†). However, in order to have a more precision measurement of an individual nanoalloy crystal,
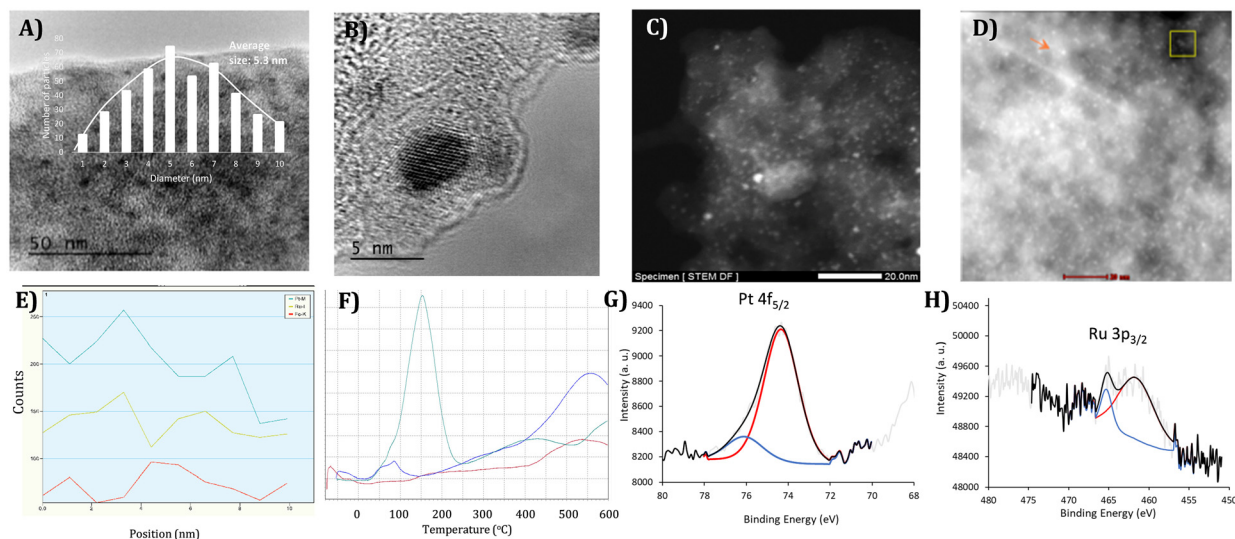

Fig. 2 A) Representative HR-TEM image of 100 nm² for RuPt–C (1:1), the inset shows the histogram taken from at least 5 different images and the calculated particle average size. B) Amplification of a RuPt nanocrystallite (1:1). C and D) Two representative STEM DF images of RuPt–C samples (1:1), the orange arrow points one typical nanoparticle. E) EDX sweeping spectra of the squared area in D), the signal for residual Fe on the support serves as a blank and follows a completely different pattern than the Ru and Pt signals. F) TPR spectra of Ru–C (blue line), Pt–C (red line) and a representative sample of RuPt–C (grey line, 1:1), after previous oxidation of the samples. G) Pt_{4f} XPS of RuPt–C (1:1). H) Ru_{3p} XPS of RuPt–C (1:1).

Table 1 Percentage of atoms in surface for the different nanoparticles supported on carbon, taken the diameter size of different nanoparticles as an average in the HR-TEM measurements, and approaching the nanoparticles to perfect nanocubes for the mathematical calculation

Entry	Catalyst	Particle diameter (d, nm)	Atoms on surface (%)
1	Ru–C	9.6	7
2	Pt–C	2.3	19
3	RuPt–C (2 : 1)	6.5	11
4	RuPt–C (1 : 1)	5.3	13
5	RuPt–C (1 : 3)	4.0	13

STEM-DF with a high-angle annular detector was employed (Fig. S5†). Spectra were collected by sweeping during just 625 ms, to avoid damaging of the nanoparticle, which was enough to observe the interaction of the nanoparticle with the electron beam despite the very low current (barely 100 pA) employed. As it can be seen, the quantification, with the atomic error measured, gives a molar Ru : Pt ratio of approximately 1 : 1. Besides, only intimate but not monometallic, shell–core or partially segregated particles could be observed. In view of the extremely good homogeneity of the nanoparticles on the material (Fig. S6†), these results strongly support the formation of intimate RuPt nanoalloys on the charcoal surface.

In order to confirm the formation of intimate RuPt nanoalloys, temperature-programmed reduction (TPR) experiments between −100 and 600 °C were performed, for Ru–C, Pt–C and RuPt–C samples, after previous oxidation under air. Fig. 2F shows that Ru needs a temperature of ≈500 °C to be reduced, Pt is extremely easy to be reduced, at ≈−50 °C, and the RuPt sample (1 : 1) shows an intermediate reduction temperature of 150 °C, with a signal in the RuO_2 reduction temperature range (450 °C) that accounts for ~15% of the total integrated area.[18] The 2 : 1 and 1 : 3 RuPt–C samples consistently gave the intermediate temperature reduction peak as the major signal, at around 150 °C (Fig.
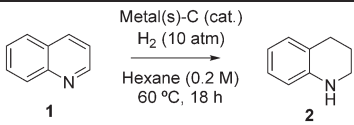
S7†). The RuO_2 signal decreases as the RuPt nanoalloy enriches in Pt, to give <10% of integrated area for pure Ru phase in the 1 : 3 RuPt–C sample. These results confirm that the three RuPt–C materials are mainly formed by intimate alloyed nanoparticles, which no more presents the chemophysical properties of the individual Ru or Pt aggregates but intermediate properties.

Fig. 2G and H shows the X-ray photoelectron spectroscopy (XPS) measurements of RuPt–C (1 : 1), with main peaks at binding energies of 74.4 and 461.6 eV for Pt $4f_{5/2}$ and Ru $3p_{3/2}$, respectively, which agrees well with both metals in zero valence state. Small contributions (around 15% for both) of 76.1 eV and 465.3 eV can be assigned to Pt^{2+} and Ru^{4+}, respectively, associated with surface species.[19]

Catalytic results

We first focused on the selective hydrogenation of quinolines, a challenging reaction in organic chemistry since the basic N atom of the aromatic ring easily poisons and deactivates metallic catalysts.[20] Table 2 shows the regioselective hydrogenation of quinoline **1** to 1,2,3,4-tetrahydroquinoline **2** in the presence of Ru–C, Pt–C or RuPt–C catalysts. While both monometallic catalysts give <50% of **2** (entries 1–4), the three different RuPt nanoalloys consistently give good yields

Table 2 Synthesis of 1,2,3,4-tetrahydroquinoline **2** by partial hydrogenation of quinoline **1**

Metal(s)-C (cat.)
H_2 (10 atm)
Hexane (0.2 M)
60 °C, 18 h

Entry	Metal	Mol%[a]	Conversion[b] (%)	Yield[b] (%)
1	Ru	1	41	25
2		10	100	48
3	Pt	1	9	0
4		10	74	35
5	RuPt (1 : 1)	1	54	41
6		10	100	68
7	RuPt (1 : 3)	1	94	83
8		10	100	80
9	RuPt (2 : 1)	1	59	44
10		10	100	64
11	RuPt (1 : 1)[c]	1	100	68
12	RuPt (1 : 1)[d]	10	100	73
13	RuPt (1 : 1)[e]	10	100	80

[a] Total amount of metals. [b] GC yield, using n-dodecane as an internal standard. [c] 10 times less metal wt% impregnated on the solid. [d] Pt impregnation first. [e] Ru impregnation first.

2510 | Catal. Sci. Technol., 2023, **13**, 2508–2516

This journal is © The Royal Society of Chemistry 2023

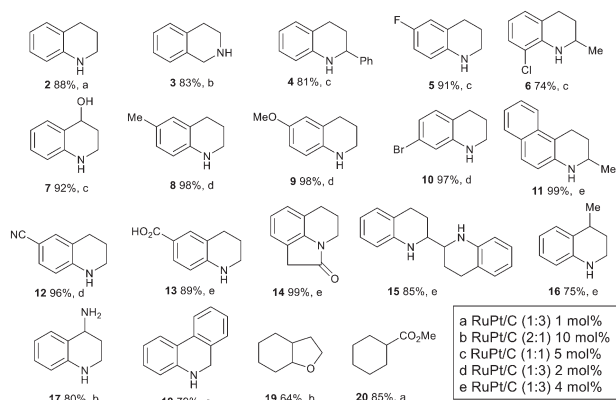**Catalysis Science & Technology**   **Paper**

Fig. 3 Hydrogenation of quinolines, isoquinolines, benzofuranes and arenes using different RuPt nanoparticles on carbon. Reaction conditions: THF (0.25 M), H$_2$ (10 atm), RuPt/C, 60 °C, 18 h. GC or NMR yield.

of **2** (44–83%, entries 6–13), regardless of the order of impregnation of the metal on the support (compare entries 10 and 12–13). The 1:3 RuPt nanoalloy proved catalytically superior to the 1:1 and 2:1 counterparts, and the total amount of metals can be decreased to 1 mol% without depletion in the final yield of **2** (entry 7). Even the amount of metals impregnated on the solid can be decreased ten times (to 0.5 wt%) without hampering the final yield, provided that a total catalytic metal amount of at least 1 mol% is employed (entry 11).

Fig. 3 shows that the different RuPt–C catalysts allow the selective hydrogenation not only of different quinolines (products **2**, **4–18**) but also of isoquinolines (product **3**), benzofuranes (product **19**) and benzoic methyl ester (product **20**),[21] in good yields and with good tolerance for halide (products **5**, **6** and **10**), alcohol (product **7**), ether (product **9**), cyano (product **12**), carboxylic acid (product

13), amide (product **14**) and ester substitutions (product **20**).

It must be noticed that the partially hydrogenated bicyclic aromatic products are stable under hydrogenating reaction conditions, and resist a further hydrogenation of the second aromatic ring. However, if the RuPt–C catalyst is active enough, it may be expected that the hydrogenation of anilines will occur under similar reaction conditions. Table 3 shows the results for the hydrogenation of nitrobenzene **21** at 60 °C in the presence of Ru–C, Pt–C or RuPt–C catalysts. Here, the nitro group should be easily hydrogenated to give aniline in one-pot. Indeed, 1 mol% of the Ru and Pt catalysts give aniline **22** as the major product (entries 1 and 2), however, the different RuPt nanoalloy compositions give the corresponding hydrogenation-coupling product, i.e. dicyclohexylamine **24**, in significant amounts, to finally achieve a 94% yield of **24** when 10 mol% of RuPt (2:1) is used (entry 8). In contrast to the hydrogenation of quinolines and derivatives, the hydrogenation-coupling reaction proceeds better with Ru-rich rather than Pt-rich nanoalloys (compare entries 5, 8 and 9). These results reflect the importance of studying different metal compositions of the supported nanoalloy in catalytic studies.

The order of impregnation of the metal in the support is not catalytically relevant (compare entries 5 and 11–12) and the amount of impregnated metal in the solid has also low impact in the results (compare entries 3 and 10). Other reaction conditions tested, which include different reaction temperatures (25 to 100 °C), solvent (dichloromethane, 1,4-dioxane, dimethylsulfoxide and water), substrate concentration (neat) and support (Al$_2$O$_3$), did not improve the results.

The superiority of RuPt nanoalloys vs. the separate metals to catalyse the hydrogenation of aniline is in line with previous literature.[6,22–24] However, the ability of RuPt–C to
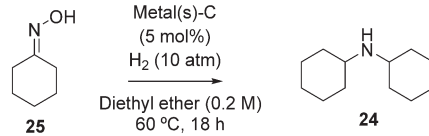
Table 3 Synthesis of dicyclohexylamine **24** by hydrogenation and amine coupling from nitrobenzene **21**. Conversion was 100% in all cases. Mass balances are completed with by-products coming from hydrogenolysis reactions

Entry	Metal	Mol%[a]	**22**[b] (%)	**23**[b] (%)	**24**[b] (%)	Selectivity to **24** (%)
1	Ru	1	99	—	—	—
2	Pt	1	92	8	—	—
3	RuPt (1:1)	1	79	—	6	79
4		5	28	2	19	28
5		10	5	2	17	17
6	RuPt (2:1)	1	41	26	33	56
7		5	67	8	25	76
8		10	—	6	94	94
9	RuPt (1:3)	10	—	12	88	88
10	RuPt (1:1)[c]	1	57	6	12	12
11	RuPt (1:1)[d]	10	45	4	11	11
12	RuPt (1:1)[e]	10	0	4	36	36

[a] Total amount of metals. [b] GC yield, using n-dodecane as an external standard. [c] 10 times less metal wt% impregnated on the solid. [d] Pt impregnation first. [e] Ru impregnation first.

Table 4 Synthesis of dicyclohexylamine **24** by hydrogenation and coupling of oxime **25**. Conversion was 100% in all cases

Entry	Catalyst	Yield[a] (%)	TOF_0[b] (h^{-1})
1	Ru–C	37	535
2	Pt–C	67	2353
3	RuPt–C (1:1)	92	4285
4	RuPt–C (2:1)	94	8300
5	RuPt–C (1:3)	89	14 250

[a] GC yield, using *n*-dodecane as an external standard. [b] Calculated as initial rate of the reaction per superficial atoms, considering perfect nanocubes (see next section).

catalyse the amine coupling is unique, and nicely complements the direct hydrogenation. With these results in hand, the coupling of other oxidized amine derivatives, in this case oximes, was attempted. Oximes have been rarely used as coupling partners in hydrogen borrowing reactions,[25] despite they are intermediates during the hydrogenation of nitrocompounds.[26] Thus, the possibility that oximes could also participate in the one-pot hydrogenation-coupling process, with the RuPt–C catalysts, was tested.

Table 4 shows that cyclohexanone oxime **25** reacts in the presence of 5 mol% of different RuPt–C samples to give dicyclohexanamine **24** in 89–94% yields, while Ru–C and Pt–C gave 37 and 67% yields, respectively. Kinetic experiments showed that the initial turnover frequency (TOF_0) for the RuPt–C catalysts approaches 10 000 h^{-1}, one order of magnitude higher than for monometallic catalysts ($\approx$500 and 2300 h^{-1} for Ru and Pt, respectively). Although it is true that the concept of TOF is questionable for nanoparticles since it considers that all the surface atoms are active during catalysis, the TOF is at least a quantitative approach to compare between different nanoparticle sizes.

Fig. 4 shows the one-pot synthesis and then reductive coupling of oximes, from aldehydes and hydroxylamine hydrochloride, to yield the symmetric secondary amines **27a–b** as coupling products in excellent yields. Since the participation of nitrobenzenes and oximes in amine coupling under hydrogenating conditions opens the door to the use of other amine precursors, nitriles were also tested,[27] and Fig. 4

also shows that they can be coupled to oximes to give amines **28a–d** and **29a–d** in reasonable yields.

The RuPt–C (1:1) catalyst could be reused up to 4 times for the coupling of cyclohexanone oxime **25**, with a decrease in the final yield from 92 to 77% yield. A hot filtration test shows that catalytically active species are not present in solution (Fig. S8†), which confirms the heterogenous nature of the catalysis but does not explain the loss of catalytic activity throughout the reuses. A possible cause for catalyst deactivation is aggregation of the nanoalloy particles during reaction. However, XRD analysis of the spent catalyst did not show any aggregation of the RuPt NPs according to the Scherrer equation (Fig. S9†). Another possible cause for catalyst deactivation is poisoning of the surface with heavily adsorbed organic products. To study this, an elemental analysis of the thoroughly washed used catalyst was performed, and it was found that the spent solid catalyst contained an additional 2.2% of nitrogen after reaction (Table S1†). Thus, the loss of catalytic activity can be ascribed to adsorbed nitrogen species derived from the reactant which, however, does not severely hamper the recyclability of the solid catalyst. It has to be noticed that while the RuPt nanoparticles are stable according to the Scherrer equation, the Ru nanoparticles agglomerate, at least to 2.5 times bigger average diameter sizes (Fig. S9†), and the latter also adsorb organic compounds (Table S1†).

Catalytic reaction mechanism

The catalytic activity of the supported nanoparticles can be referred to the surface atoms, in contact with the reagents. Thus, the % of surface atoms for each catalyst was calculated (Fig. S10†). For that, the following formula was employed: $d = 1.105 \times 0.29 \times N_{total}^{1/3}$, where the diameter of the nanoparticle (d, obtained from HR-TEM experiments) was used to calculate the number of total atoms (N_{total}) in the (Ru)Pt nanoparticle. The approach of considering nanocubes instead of circular particles facilitates the calculation and does not give much error for small nanoparticles, as it is our case here. With values taken from typical crystallographic
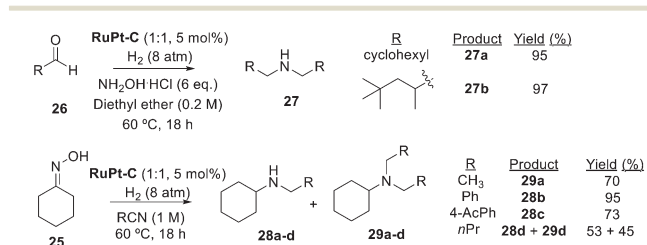

Fig. 4 One-pot synthesis of secondary and tertiary amines catalysed by RuPt–C (1:1) from aldehydes **26** and hydroxylamine chloride (top), and from oxime **25** and nitriles (bottom).

distances for Ru and Pt, the % of atoms in surface for each catalyst could be calculated. The results are shown in Table 1, above. With these data in hand, the turnover frequencies for the individual reactions and catalysts can now be calculated, since initial rates for each solid catalyst are addressed from the initial points in the corresponding kinetic curve, where the particle size should still be maintained, at least in a first approximation. To check this, the RuPt–C (1 : 1) solid was treated with an atmosphere of H_2 in the pre-chamber of the XPS instrument, at 60 °C for 1 h (Fig. S11†). The main peaks observed for Ru in the RuPt–C (1 : 1) sample before treatment appear at 460.0 eV (8%) and 461.6 eV (75%) for Ru, that corresponds to Ru^0 and $Ru^{\delta+}$, respectively, and at 74.3 eV for Pt, which corresponds to Pt^0 (85%). Despite the amplitude of the signals, it can be considered that the Ru 3p and Pt 4f peaks are mainly unmodified after H_2 treatment, which confirms that the RuPt–C (1 : 1) catalyst keeps the observed structure under the catalytic hydrogenation reactions.

Then, we studied the hydrogenation reaction with a variety of aromatic molecules. First, three aromatic rings with very different electron density (anisole, *tert*-butylbenzene and trifluoromethylbenzene; Table S2 and Fig. S12†) were tested.[28] It was found that the richer Pt nanoalloys, *i.e.* RuPt (1 : 3), were the more active catalysts, despite Pt–C was merely inactive. Notice that not only Ru–C and Pt–C by separate, were low active for the reaction, but also a physical mixture of Ru–C and Pt–C was also inactive. The low catalytic activity observed for the Ru/C catalyst can be explained by a partial oxidation on surface, which is easy considering the slow size of the crystallites and is in accordance with the XPS measurements. Without Pt in the nanoparticle, H_2 splitting should be more difficult. Regarding substrate substitution, the different RuPt–C catalysts roughly obey the Taft rule, *i.e.* aromatic rings with bulky substituted groups reacts sluggishly due to steric constraints on the extended metal surface, as assessed here with *tert*-butylbenzene (see Table S2†). This result further proves the heterogeneous nature of the catalyst, in accordance with the classical Horiuti–Polanyi mechanism for the hydrogenation of aromatics on metal surfaces.[29] A second study on the aromatic hydrogenation reaction was performed with acetophenone as a substrate (Tables S3–S5 and Fig. S13†), where it was found again that the RuPt nanoalloy (1 : 3) was much more catalytically active than the Ru-richer Pt nanoalloys and also than the monometallic counterparts, achieving complete hydrogenation of the substrate. A third study was performed with *para*-vinyl benzoic acid, a substrate containing alkene, aromatic and carboxylic acid functionalities (Table S6†). The results showed that the alkene functionality is much more rapidly hydrogenated than the arene ring on the RuPt–C (1 : 1) nanoalloy catalyst, while the carboxylic acid remains unreacted. These results prove that the catalytic activation of the organic functional group controls the reaction rate, and that H_2 dissociation easily occurs on the RuPt–C nanoalloy. Overall, the results on the hydrogenation of different arene
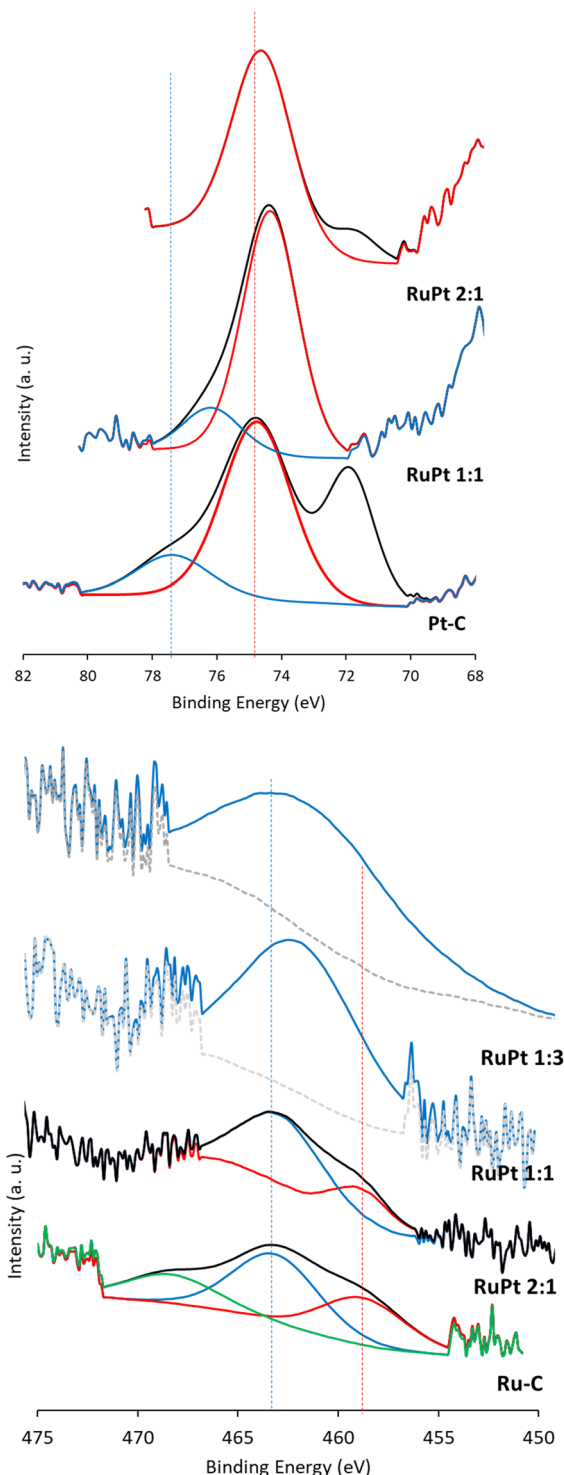

Fig. 5 Deconvoluted Pt_{4f} (top) and Ru_{3p} (bottom) XPS measurements of the different solid catalysts, showing the electron transfer from Ru to Pt. For Pt, a shift to lower binding energies is found (more electron rich). For Ru, a shift to higher binding energies is found (more electron poor). Lines are a guide to the eye. Notice that the Pt 4f signal for the RuPt–C (1 : 3) alloy is not shown since residual pure Pt nanoparticles shift the signal to higher binding energies. Regarding the Ru signals, the alloy RuPt–C 1 : 1 does not show any metallic Ru signal, as it can be somewhat observed in the RuPt–C 2 : 1 alloy.

This journal is © The Royal Society of Chemistry 2023

Catal. Sci. Technol., 2023, **13**, 2508–2516 | **2513**

rings support the key role of nanoalloyed Pt as the more active metal for the catalysis.

Then, the hydrogen-borrowing coupling reaction of **22** was studied (Table S7†). It was found that Ru–C was very active in forming product **23**, but not **24**, if a stoichiometric amount of cyclohexylamine is added to the reaction mixture. The fact that product **23** (aromatic–aliphatic) is exclusively formed with the Ru–C catalyst, and not product **24** (aliphatic–aliphatic), and that cyclohexylamine is required for the coupling to proceed, strongly supports that Ru sites are mainly involved in the coupling but not in the hydrogenation reaction. In accordance, Pt–C is totally inactive for the coupling reaction under the same reaction conditions, while the RuPt–C (1:1) nanoalloy catalyst gives the fully hydrogenated product **24**. These results corroborate that Ru metal atoms mainly constitute the active metal sites for the hydrogen-borrowing coupling reaction.

The above catalytic results and conclusions are in line with the expected electronic properties of the Pt and Ru atoms in the RuPt nanoalloy. Pt is more electronegative than Ru, and since both are in formal zero oxidation state, Pt removes some electron density from Ru to get itself slightly more electron rich, while Ru gets more electron poor within the intimate nanoalloy. The value of relative electron density transferred from Ru to Pt has been calculated to be ~0.04 e^{-}.[30] Thus, in one hand, nanoalloyed Pt is more prone to dissociate H_2 through transferring of electron density to the antibonding σ* orbital of H_2, then facilitating hydrogenation reactions. And in the other hand, nanoalloyed Ru is slightly more cationic to coordinate and activate the C–N bonds of the amine, thus manifolding the hydrogen-borrowing coupling. XPS measurements of the different RuPt–C solids confirm the electronic transferring of Ru to Pt.[31] Fig. 5 shows that lower and higher binding energies values for Pt and Ru, respectively, can be found in the different RuPt nanoalloys, compared to the monometallic materials. For instance, the peaks corresponding to Pt 4f decrease in their binding energy (from 74.7 to 74.4 eV and from 77.3 to 76.0 eV, respectively) with the amount of Pt. Thus, one can say that electron poorer Ru atoms and electron richer Pt atoms are present in the nanoalloy.

Fig. 6 shows a plausible general mechanism for the hydrogenation and the one-pot hydrogenation and coupling reactions with intimate nanoalloyed RuPt–C catalysts.[12] The oxidised alkyl or aromatic amine undergoes hydrogenation to primary alkyl amines over Pt sites on the catalyst. The hydrogenated molecule then participates in the hydrogen-borrowing event on the Ru sites of the catalyst, to give the corresponding secondary amine. Further hydrogenation can then occur, again on Pt sites. Depending on steric effects, the secondary amine can suffer, or not, a last dehydrogenation and coupling to form the tertiary amine. Alternatively, the secondary amine can attack a primary imine formed by dehydrogenation of the primary amine to form the tertiary amine. This mechanism is supported by the formation of the coupling product **24** when starting the reaction either from aniline **22** or cyclohexylamine, and also by the confirmation by gas-chromatography coupled to mass-spectrometry (GC-MS) that NH_3 appears as a major by-product during reaction.

Conclusions

RuPt nanoalloys supported on charcoal outperform the catalytic activity of monometallic Ru–C and Pt–C nanoparticles for the synthesis of secondary and tertiary amines from oxidized amine derivatives, under a hydrogen atmosphere. The solid catalyst is truly heterogeneous and recyclable. These results may stimulate new studies on nanoalloys as catalysts for complex organic synthesis, likely superior compared to monometallic counterparts, especially in tandem reactions.

Author contributions

M. A. R.-C. performed and analysed the data of the catalytic tests; P. R.-M. synthesized and characterized the materials and performed some catalytic experiments; J. C. H.-G. carried out and interpreted the HAADF-STEM analyses of individual RuPt/C (1:1) nanoparticles; M. M. and J. O.-M. performed and interpreted some characterization to establish the catalyst structure–activity relationship; A. L.-P. conceived and coordinated the work, supervised the synthetic and catalytic part, and wrote the manuscript.

Conflicts of interest

There are no conflicts to declare.
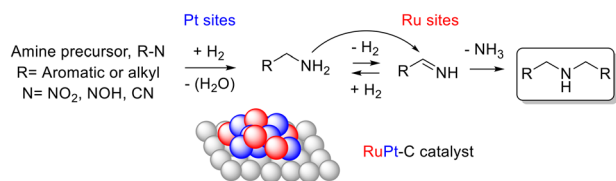
Acknowledgements

Fig. 6 Proposed reaction mechanism for the hydrogenation and one-pot hydrogenation-coupling of nitrocompounds, oximes and/or nitriles, over RuPt–C catalysts and under a H_2 atmosphere.

2514 | *Catal. Sci. Technol.*, 2023, **13**, 2508–2516

This journal is © The Royal Society of Chemistry 2023

Notes and references

1 (a) P. K. Gupta and L. Mishra, *Nanoscale Adv.*, 2020, **2**, 1774–1791; (b) M. M. Seitkalieva, D. E. Samoylenko, K. A. Lotsman, K. S. Rodygin and V. P. Ananikov, *Coord. Chem. Rev.*, 2021, **445**, 213982.

2 (a) S. Alayoglu, A. U. Nilekar, M. Mavrikakis and B. Eichhorn, *Nat. Mater.*, 2008, **7**, 333–338; (b) M. J. S. Farias, W. Cheuquepan, A. A. Tanaka and J. M. Feliu, *ACS Catal.*, 2017, **7**, 3434–3445; (c) P. Zhou, X. Hou, Y. Chao, W. Yang, W. Zhang, Z. Mu, J. Lai, F. Lv, K. Yang, Y. Liu, J. Li, J. Ma, J. Luo and S. Guo, *Chem. Sci.*, 2019, **10**, 5898–5905.

3 (a) Z. Yang, D. Yang, Y. Wang, Y. Long, W. Huang and G. Fan, *Nanoscale*, 2021, **13**, 10044–10050; (b) S. Zhu, X. Qin, F. Xiao, S. Yang, Y. Xu, Z. Tan, J. Li, J. Yan, Q. Chen, M. Chen and M. Shao, *Nat. Catal.*, 2021, **4**, 711–718.

4 (a) M. Bello, S. M. J. Zaidi, A. Al-Ahmed, S. Basu, D.-H. Park, K. S. Lakhi and A. Vinu, *Microporous Mesoporous Mater.*, 2017, **252**, 50–58; (b) S. Xue, W. Deng, F. Yang, J. Yang, I. S. Amiinu, D. He, H. Tang and S. Mu, *ACS Catal.*, 2018, **8**, 7578–7584; (c) J. Zhang, X. Qu, Y. Han, L. Shen, S. Yin, G. Li, Y. Jiang and S. Sun, *Appl. Catal., B*, 2020, **263**, 118345; (d) Q. Wang, S. Chen, J. Jiang, J. Liu, J. Deng, X. Ping and Z. Wei, *Chem. Commun.*, 2020, **56**, 2419–2422; (e) G. Montiel, E. Fuentes-Quezada, M. M. Bruno, H. R. Corti and F. A. Viva, *RSC Adv.*, 2020, **10**, 30631–30639; (f) Q. Wang, S. Chen, P. Li, S. Ibraheem, J. Li, J. Deng and Z. Wei, *Appl. Catal., B*, 2019, **252**, 120–127; (g) A. Torres, H. Shi, B. Subramaniam and R. V. Chaudhari, *ACS Sustainable Chem. Eng.*, 2019, **7**, 11323–11333.

5 For reviews see: (a) R. A. Adams and B. Captain, *J. Organomet. Chem.*, 2004, **689**, 4521–4529; (b) E. Antolini, *J. Solid State Electrochem.*, 2011, **15**, 455–472.

6 (a) L. Zhu, S. Shan, V. Petkov, W. Hu, A. Kroner, J. Zheng, C. Yu, N. Zhang, Y. Li, R. Luque, C.-J. Zhong, H. Ye, Z. Yang and B. H. Chen, *J. Mater. Chem. A*, 2017, **5**, 7869–7875; (b) L. Zhu, H. Zhang, W. Hu, J. Zheng, N. Zhang, C. Yu, H. Ye, Z. Yang and B. H. Chen, *ChemCatChem*, 2018, **10**, 1998–2002; (c) L. Zhu, H. Zhang, N. Ma, C. Yu, N. Ding, J.-L. Chen, C.-W. Pao, J.-F. Lee, Q. Xiao and B. H. Chen, *J. Catal.*, 2019, **377**, 299–308.

7 (a) A. Weilhard, G. Abarca, J. Viscardi, M. H. G. Prechtl, J. D. Scholten, F. Bernardi, D. L. Baptista and J. Dupont, *ChemCatChem*, 2017, **9**, 204–211; (b) Y. Xu, C. Wu, Y. Wang, Y. Zhang, H. Sun, H. Chen and Y. Zhao, *Chin. Chem. Lett.*, 2021, **32**, 516–520.

8 L. A. Oro, D. Carmona and J. M. Fraile, in *Metal–catalysis in Industrial Organic Processes*, The Royal Society of Chemistry, 2006, pp. 79–113.

9 For a review with relevant patents see: K. S. Hayes, *Appl. Catal., A*, 2001, **221**, 187–195 and references therein.

10 For reviews see: (a) M. H. S. A. Hamid, P. A. Slatford and J. M. J. Williams, *Adv. Synth. Catal.*, 2007, **349**, 1555–1575; (b) T. D. Nixon, M. K. Whittlesey and J. M. J. Williams, *Dalton Trans.*, 2009, 753–762; (c) G. Guillena, D. J. Ramon and M. Yus, *Chem. Rev.*, 2010, **110**, 1611–1641; (d) G. E. Dobereiner and R. H. Crabtree, *Chem. Rev.*, 2010, **110**, 681–703.

11 For reviews see: (a) P. Serna and A. Corma, *ACS Catal.*, 2015, **5**, 7114–7121; (b) A. Corma, J. Navas and M. J. Sabater, *Chem. Rev.*, 2018, **118**, 1410–1459; (c) E. Podyacheva, O. I. Afanasyev, D. V. Vasilyev and D. Chusov, *ACS Catal.*, 2022, **12**, 7142–7198.

12 For some references see: (a) Y. Yamane, X. Liu, A. Hamasaki, T. Ishida, M. Haruta, T. Yokoyama and M. Tokunaga, *Org. Lett.*, 2009, **11**, 5162–5165; (b) L. L. Santos, P. Serna and A. Corma, *Chem. – Eur. J.*, 2009, **15**, 8196–8203; (c) A. Corma, T. Rodenas and M. J. Sabater, *Chem. – Eur. J.*, 2010, **16**, 254–260; (d) P. Rubio-Marques, A. Leyva-Perez and A. Corma, *Chem. Commun.*, 2013, **49**, 8160–8162; (e) S. G. Oh, V. Mishra, J. K. Cho, B.-J. Kim, H. S. Kim, Y.-W. Suh, H. Lee, H. S. Park and Y. J. Kim, *Catal. Commun.*, 2014, **43**, 79–83; (f) P. Rubio-Marques, J. C. Hernandez-Garrido, A. Leyva-Perez and A. Corma, *Chem. Commun.*, 2014, **50**, 1645–1647.

13 For some references see: (a) H.-U. Blaser and M. Studer, *Acc. Chem. Res.*, 2007, **40**, 1348–1356; (b) H.-U. Blaser, H. Steiner and M. Studer, *ChemCatChem*, 2009, **1**, 210–221.

14 For some reviews see: (a) A. Stanislaus and B. H. Cooper, *Catal. Rev.: Sci. Eng.*, 1994, **36**, 75–123; (b) S.-C. Qi, X.-Y. Wei, Z.-M. Zong and Y.-K. Wang, *RSC Adv.*, 2013, **3**, 14219–14232; (c) P. Lara, K. Philippot and B. Chaudret, *ChemCatChem*, 2013, **5**, 28–45.

15 For some representative references see: (a) T. Maegawa, A. Akashi, K. Yaguchi, Y. Iwasaki, M. Shigetsura, Y. Monguchi and H. Sajiki, *Chem. – Eur. J.*, 2009, **15**, 6953–6963; (b) M. Zahmakiran, Y. Tonbul and S. Oezkar, *Chem. Commun.*, 2010, **46**, 4788–4790; (c) M. Fang and R. A. Sanchez-Delgado, *J. Catal.*, 2014, **311**, 357–368.

16 For some representative references see: (a) D. Hollmann, S. Bahn, A. Tillack and M. Beller, *Angew. Chem., Int. Ed.*, 2007, **46**, 8291–8294; (b) A. Tillack, D. Hollmann, K. Mevius, D. Michalik, S. Bahn and M. Beller, *Eur. J. Org. Chem.*, 2008, 4745–4750; (c) J. He, J. W. Kim, K. Yamaguchi and N. Mizuno, *Angew. Chem., Int. Ed.*, 2009, **48**, 9888–9891; (d) D. Pingen, C. Muller and D. Vogt, *Angew. Chem., Int. Ed.*, 2010, **49**, 8130–8133; (e) M. Mon, R. Adam, J. Ferrando-Soria, A. Corma, D. Armentano, E. Pardo and A. Leyva-Pérez, *ACS Catal.*, 2018, **8**, 10401–10406.

17 R. Ferrando, J. Jellinek and R. L. Johnston, *Chem. Rev.*, 2008, **108**, 845–910.

18 S.-Y. Huang, S.-M. Chang and C. Yeh, *J. Phys. Chem. B*, 2006, **110**, 234–239.

19 E. A. Anumol, A. Halder, C. Nethravathi, B. Viswanath and N. Ravishankar, *J. Mater. Chem.*, 2011, **21**, 8721–8726.

20 D. Ren, L. He, L. Yu, R.-S. Ding, Y.-M. Liu, Y. Cao, H.-Y. He and K.-N. Fan, *J. Am. Chem. Soc.*, 2012, **134**, 17592–17598.

21 A. Karakulina, A. Gopakumar, I. Akcok, B. L. Roulier, T. LaGrange, S. A. Katsyuba, S. Das and P. J. Dyson, *Angew. Chem., Int. Ed.*, 2016, **55**, 292–296.

This journal is © The Royal Society of Chemistry 2023

Catal. Sci. Technol., 2023, **13**, 2508–2516 | **2515**

22 For a review see: J. M. Thomas, B. F. G. Johnson, R. Raja, G. Sankar and P. A. Midgley, *Acc. Chem. Res.*, 2003, **36**, 20–30.

23 For seminal works see: G. C. Bond and D. E. Webster, *Proc. Chem. Soc., London*, 1964, 398.

24 For a represenative reference see: N. A. Dehm, X. Zhang and J. M. Buriak, *Inorg. Chem.*, 2010, **49**, 2706–2714.

25 (*a*) M. Searcey, S. S. Grewal, F. Madeo and P. G. Tsoungas, *Tetrahedron Lett.*, 2003, **44**, 6745–6747; (*b*) E. Gebauer-Henke, W. Leitner, A. Prokofieva, H. Vogt and T. E. Mueller, *Catal. Sci. Technol.*, 2012, **2**, 2539–2548.

26 A. Corma, P. Serna and H. Garcia, *J. Am. Chem. Soc.*, 2007, **129**, 6358–6359.

27 (*a*) H. Sajiki, T. Ikawa and K. Hirota, *Org. Lett.*, 2004, **6**, 4977–4980; (*b*) R. Nacario, S. Kotakonda, D. M. D. Fouchard, L. M. V. Tillekeratne and R. A. Hudson, *Org. Lett.*, 2005, **7**, 471–474.

28 X. Cui, A.-E. Surkus, K. Junge, C. Topf, J. Radnik, C. Kreyenschulte and M. Beller, *Nat. Commun.*, 2016, **7**, 11326.

29 G. S. Fonseca, E. T. Silveira, M. A. Gelesky and J. Dupont, *Adv. Synth. Catal.*, 2005, **347**, 847–853.

30 M. Harada and H. Dexpert, *J. Phys. Chem.*, 1996, **100**, 565–572.

31 S. Alayoglu, P. Zavalij, B. Eichhorn, Q. Wang, A. I. Frenkel and P. Chupas, *ACS Nano*, 2009, **3**, 3127–3137.